Elena G. Astafurova[a], Irina V. Kireeva[a], Yuriy I. Chumlyakov[a], Hans J. Maier[b], Huseyin Sehitoglu[c]

[a] Laboratory of strength physics and plasticity, Siberian Physical Technical Institute, Tomsk, Russia
[b] Lehrstuhl für Werkstoffkunde, University of Paderborn, Paderborn, Germany
[c] Department of Mechanical and Industrial Engineering, University of Illinois, Urbana-Champaign, IL, USA

The influence of orientation and aluminium content on the deformation mechanisms of Hadfield steel single crystals

The low stacking fault energy and high carbon content in Hadfield steel make twinning the basic deformation mechanism from the onset of plastic deformation in [$\bar{1}$11] and [011] oriented single crystals in tension at T = 77–300 K. Alloying with aluminium (2.7 Al in wt.%) results in an increase of stacking fault energy from $0.03\ \mathrm{J \cdot m^{2}}$ to $0.05\ \mathrm{J \cdot m^{-2}}$ and moves twinning to higher degrees of deformation ($\varepsilon_{pl} > 15\,\%$). In aluminium-free [$\bar{1}$23] crystals twinning starts after 20 % strain. For [$\bar{1}$23], [001] orientations, aluminium additions change the dislocation arrangement from a uniform distribution to a planar dislocation arrangment and also suppress twinning. Intersections of dislocation pile-ups were found to be the governing factor for hardening in the aluminium-alloyed [001] crystals.

Keywords: Hadfield steel; Microstructure; Single crystal; Stacking fault energy; Twinning

1. Introduction

Hadfield manganese steel (Fe-13Mn-1.3C, in wt.%) is well known and widely used due to its anomalous high work hardening, ductility, and strength [1–5]. Quenched polycrystals of Hadfield steel have a low stacking fault energy ($\gamma_{SF} = 0.030\ \mathrm{J \cdot m^{-2}}$ [1]) and exhibit mechanical twinning in a wide range of test temperatures (T = 77 K – 473 K). There are two main reasons for the high work hardening of Hadfield steel. Firstly, twinning is believed to contribute to the high values of the strain-hardening coefficient $\theta = \mathrm{d}\sigma/\mathrm{d}\varepsilon_{pl}$ (σ – applied stresses, ε_{pl} – plastic strain) due to twin–twin or twin–slip intersection. In turn, the resulting refinement of the microstructure by numerous twins and stacking faults hinders dislocation motion [1–3]. Secondly, the high rate of strain hardening is often also ascribed to the high content of carbon, and gives rise to dynamic strain-ageing phenomena. Strain ageing is thought to be the primary cause for the accumulation of glide dislocations in planar arrangements, and is accompanied by serrated flow and a negative strain rate dependence in the temperature interval 240 K to 525 K [4]. For Hadfield steel, the latter effect is attributed to the destruction and restoration of short-range order when glide dislocations encounter Mn–C pairs [5]. Moreover, it has been reported that alloying of a polycrystalline Hadfield steel with aluminium resulted in suppression of twinning and a positive strain-rate dependence at room temperature. Dynamic strain-ageing phenomena were also suppressed [6]. In summary, twinning, dislocation slip and strain-ageing phenomena all contribute to the stress–strain response in Hadfield steel. The relevance of the individual effects is, however, not clearly understood. The objective of the present study was to shed light on the details governing the deformation behaviour. Single crystals of Hadfield steel loaded in tension along the [001], [011], [$\bar{1}$11], and [$\bar{1}$23] directions were employed. In this manner, the Schmid factors for twinning and dislocation slip could be varied systematically.

In addition, alloying of Hadfield steel single crystals with aluminium allowed investigation of the deformation behaviour under conditions where the activity of carbon atoms is reduced compared to aluminium-free steel.

2. Experimental

Single crystals of Hadfield steel Fe-13Mn-1.3C (referred to as steel I) and Fe-13Mn-2.7Al-1.3C (steel II) (wt.%) were grown by the Bridgman technique in an inert gas atmosphere. All crystals were then homogenised in an argon atmosphere at 1373 K for 24 hours. Electro-discharge machining was utilised to cut regular dog-bone shaped flat tensile specimens with nominal dimensions of 12 mm × 3 mm × 1.5 mm in the gauge section. The tensile specimens were solution-treated at 1373 K for 1 hour and then water-quenched. Finally, grinding and an electrochemical polish (50 g CrO_3, in 200 g H_3PO_4) were employed to remove any processing-affected surface layer. Tensile tests were conducted in the temperature interval of 77 – 673 K at a strain rate of $4 \times 10^{-4}\ \mathrm{s^{-1}}$. In order to characterise the microstructural changes occurring during deformation, tensile tests were interrupted at given strains, and electron transparent foils were prepared from those samples by conventional twin-jet electropolishing.

For microstructural analysis, a Philips CM 200 transmission electron microscope (TEM) operated at 200 kV was employed.

In addition, orientation of the crystal axis and its variation (precession) during deformation were determined on a DRON-3M X-ray diffractometer for strain increments of 5 %. If one assumes that a single system is operational, the measured changes in orientation of the crystal axis (rotation) can be converted into a strain using the relation

$$\varepsilon_{\mathrm{rot}} = \frac{\sin \lambda_0}{\sin \lambda} - 1 \qquad (1)$$

where λ_0 and λ are the angles between the shear system (dislocation slip or twinning) direction, and the crystal orientation before and after deformation, respectively [7].

3. Results

Figures 1 and 2 display the stress vs. plastic strain ($\sigma - \varepsilon_{\mathrm{pl}}$) curves for steels (I) and (II) and corresponding changes of crystal axis (precession) during tensile deformation for single crystals of [011] and [$\bar{1}$11] orientation at 190 K and 300 K. Figures 3 and 4 demonstrate the microstructural evolution during deformation of [011] and [$\bar{1}$11]-oriented crystals of steels (I) and (II) after tensile deformation at 300 K and 190 K. As revealed by X-ray analysis of crystal

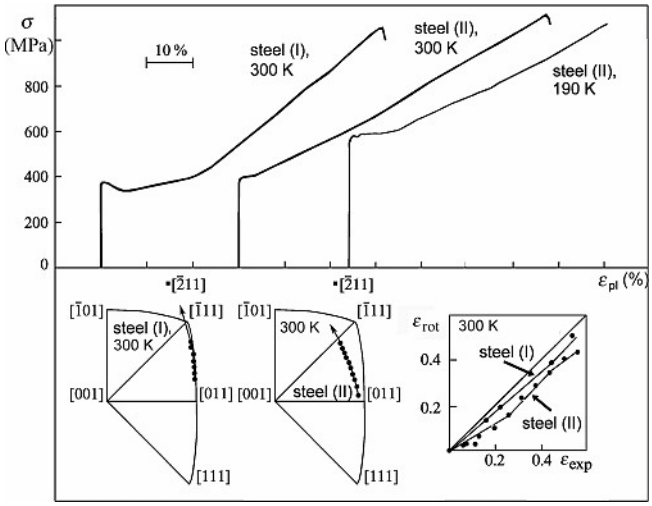

Fig 1. Stress vs. plastic strain and rotation of crystal loading axis for [011] oriented crystals. The inset shows plastic strain values as obtained by extensometry ($\varepsilon_{\mathrm{exp}}$) compared to data computed from X-ray measurements ($\varepsilon_{\mathrm{rot}}$).

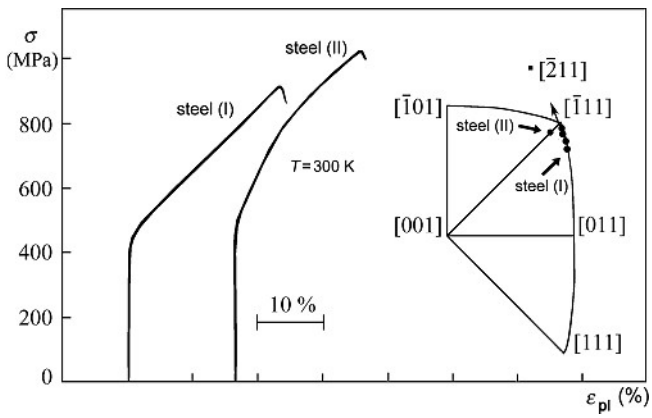

Fig. 2. Stress vs. plastic strain and rotation of the crystal loading axis for [$\bar{1}$11] oriented single crystals from steels (I) and (II) at 300 K.

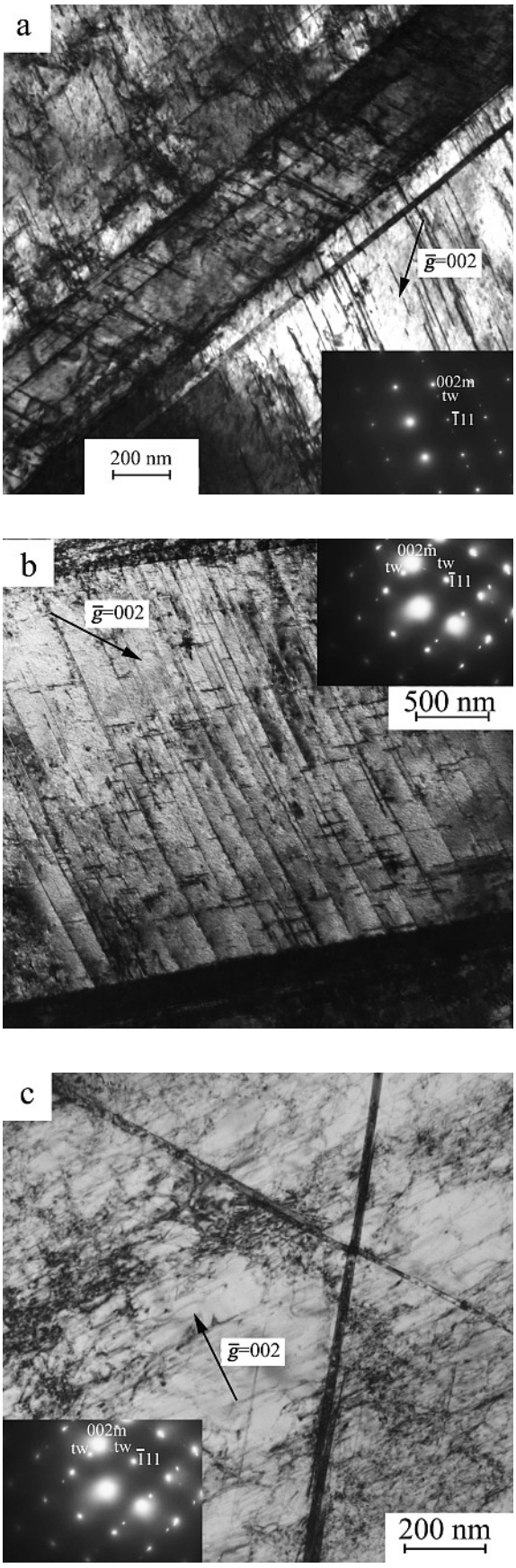

Fig. 3. TEM two-beam bright-field images showing representative microstructures observed in single crystals of steel (I) after tensile deformation at 300 K; twin (tw) and matrix (m) reflections are indicated in the corresponding selected area diffraction patterns. (a) [011], $\varepsilon_{\mathrm{pl}}$ = 5 %; (b) [011], $\varepsilon_{\mathrm{pl}}$ = 20 %; (c) [$\bar{1}$11], $\varepsilon_{\mathrm{pl}}$ = 15 %.

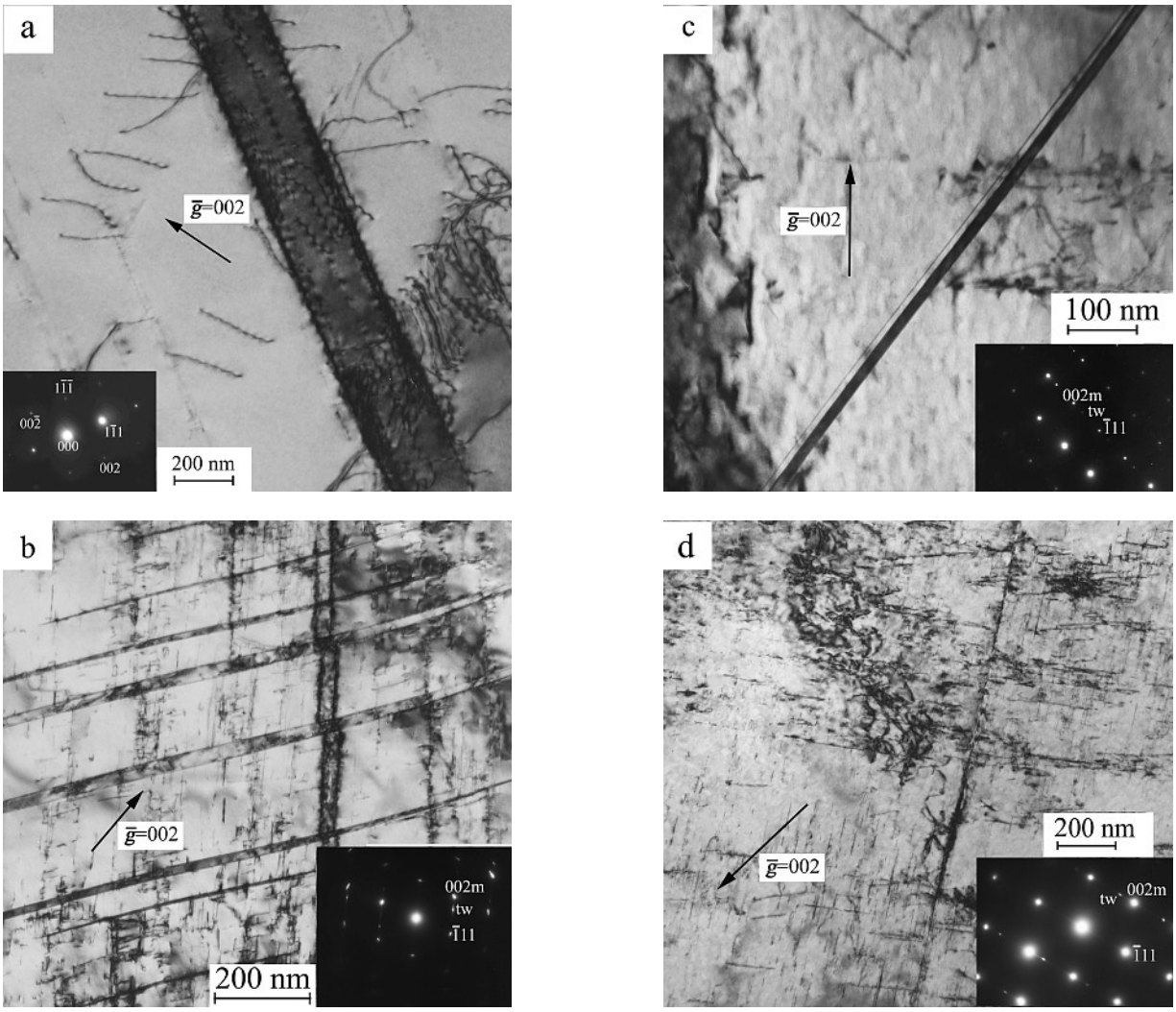

Fig. 4. Microstructural evolution during tensile deformation of steel (II). (a) [011], ε_{pl} = 5 %, T = 300 K; (b) [011], ε_{pl} = 15 %, T = 300 K; (c) [$\bar{1}$11], ε_{pl} = 10 %, T = 300 K; (d) [011], ε_{pl} = 5 %,T = 190 K.

axis rotation (Fig. 1) and TEM analysis (Fig. 3a), mechanical twinning sets in from the very beginning of plastic deformation, $\varepsilon_{pl} > 0.5$ % for the [011]-oriented crystal of steel (I). Moreover, deformation occurred initially in Lüders bands for [011]-oriented crystals, when twinning on the primary system [$\bar{2}$11](111) was the governing deformation mechanism. At larger strains ($\varepsilon_{pl} > 20$ %), twinning on the conjugate system started, and the intersection of primary and secondary twin systems (Fig. 3b) leads to a linear stress–strain $\sigma(\varepsilon_{pl})$-dependence during the second stage of the plastic flow curve (Fig. 1). The tensile axis of both the [011]- and the [$\bar{1}$11]-oriented crystals of steel (I) tend to rotate toward the [$\bar{2}$11] pole along the big circle connecting the [$\bar{2}$11] pole and the initial crystal orientation of the virgin specimens (Fig. 1). Hence, the contribution of the conjugate twin systems to overall strain is small, but it is significant with respect to the hardening behaviour of the crystals. This is most evident from the stress–strain response of the [$\bar{1}$11]-oriented crystal of steel (I) (Fig. 2), where the strain-hardening coefficient θ initially is as high as in the [011]-oriented crystals during the second stage of deformation. This is attributed to the action of multiple twinning (Fig. 3c). The comparison of strain measured by conventional extensometry (ε_{exp}) with values calculated from crystal axis precession, ε_{rot}, shows that shear is mainly dominated by one twin system [$\bar{2}$11](111) and shear loss due to the secondary twin system is of the order of 15 % (Fig. 1). For [011]-oriented crystals of steel (II) mechanical twinning is not observed during the early stages of plastic flow. Deformation proceeds by the activation of several slip systems, and dislocations form pile-ups that transform later to multipoles (Fig. 4a). The high values of the strain-hardening coefficient θ are the result of multipole intersections on several slip systems. At larger strains ($\varepsilon_{pl} > 15$ %) twinning is observed (Fig. 4b), but θ does not change compared to lower strains, i. e. $\varepsilon_{pl} < 15$ % (Fig. 1). The most plausible reason is that twinning does not act as the primary deformation mechanism at $\varepsilon_{pl} \sim 15-20$ %, and thus, the volume fraction of twins is not high. Consequently, strain hardening is still basically defined by interaction of pile-ups and multipoles.

For the aluminium-alloyed steel II, stacking fault energy (γ_{SF}) was estimated using the method of triple dislocation nodes of dislocation cells [8]. The measurements showed that alloying with aluminium leads to an increase of γ_{SF} from 0.03 J · m^{-2} to 0.050 ± 0.005 J · m^{-2}. The rise of γ_{SF} in steel (II) compared to steel (I) is assumed to be the main reason for the shift of the onset of twinning to larger plastic

Table 1. Schmid factors for slip m_{slip} and twinning $m_{twinning}$ via intrinsic stacking fault formation.

	$[\bar{1}11]$	[011]	$[\bar{1}23]$	[001]
m_{slip}	0.27	0.41	0.45	0.41
$m_{twinning}$	0.31	0.47	0.45	0.24

strains in steel (II). As the Schmid factors for twinning in $[\bar{1}11]$-oriented crystals is higher than for slip (Table 1), twinning sets in earlier (ε_{pl} = 10 %, see Fig. 4c) than in [011]-oriented single crystals of steel (II). This was proved by extensive TEM investigations of dislocation arrangements in $[\bar{1}11]$- and [011]-oriented single crystals of steel (II): no twins were observed in [011]-oriented crystals up to strains of ε_{pl} =15 %, and thin twins of one system were the distinctive feature of the microstructure in $[\bar{1}11]$ crystals at $\varepsilon_{pl} \geq 10\,\%$ (Fig. 4c) and in [011] crystals at $\varepsilon_{pl} \geq 15\,\%$ (Fig. 4b). A low temperature test on [011]-oriented samples of steel (II) demonstrated that a decrease in the temperature moves the onset of twinning to earlier stages of plastic deformation, i.e. twinning was observed $\varepsilon_{pl} = 3-5\,\%$ (Fig. 4d).

In Figs. 5 and 6, $\sigma-\varepsilon_{pl}$ curves and the change of crystal axis orientation during deformation are shown for $[\bar{1}23]$ and [001] oriented crystals of steel (I) and (II). In single crystals of steel (I) plastic deformation takes place in two stages: the first linear one is associated with dislocation slip, the second with the interaction of dislocation slip and twinning (Fig. 5). Initially, deformation occurs via dislocation slip on the primary system and no twins are observed. During the second stage, the governing deformation mechanism changes from dislocation slip to twinning (Figs. 5 and 7a), which is accompanied by a substantial increase in the strain-hardening coefficient. A decrease in test temperature results in the appearance of twinning from the very beginning of plastic deformation (Figs. 5 and 7b). By contrast, dislocation slip dominates the plastic deformation of $[\bar{1}23]$ oriented crystals of steel (II). At $\varepsilon_{pl} \leq 10\,\%$, nucleation and propagation of Lüders bands occurs, then the linear hardening stage follows (Fig. 5).

Comparison of conventionally obtained strain data with those calculated from crystal axis rotation show that deformation of steel (I) and steel (II) is initially governed by dislocation slip on the primary system $[\bar{1}01](111)$ (Fig. 5).

The different microstructures formed during tensile deformation of steel (I) and (II) are manifested macroscopically via significantly different strain-hardening coefficients. Optical microscopy revealed coarse slip lines in steel (II), whereas in steel (I) the distribution of slip activity was uniform and a few slip lines were observed at $\varepsilon_{pl} <$ 10 – 15 %. Fine slip lines are rather difficult to observe on the surface of the specimens using optical microscopy. TEM investigations also indicated the presence of planar dislocation arrangements at $\varepsilon_{pl} \leq 10-15\,\%$ in all investigated orientations of steel (II), and numerous dislocation pile-ups and multipoles were also present (Fig. 7c). In steel (I) dislocation pile-ups were not observed, and the initially uniform dislocation arrangement transformed into a cellular one upon continued deformation [9, 10].

In [001] oriented crystals of steel (II) high strain hardening results from the interaction of multiple slip – pile-ups and multpoles (Fig. 7d). Twinning starts in [001]-oriented crystals of steel (I) at ε_{pl} = 3 – 5 % [9, 11]. In steel (I), interaction of dislocation slip and twinning occurs simultaneously (Fig. 7e) [9, 11].

4. Discussion

According to the results on twinning development in single crystals obtained earlier for pure metals with low stacking fault energy [12], one expects the onset of twinning in tension for loading axis orientations close to the $[\bar{1}11]$ pole. Usually, fcc metals do not, however, undergo twinning in tension for crystals oriented close to the [001] pole, even if they possess a low stacking fault energy [12]. Thus, the observed twinning of the [001]-oriented crystals of steel (I) requires an additional analysis. In pure metals and low stacking fault energy alloys, dislocation slip always precedes twinning, and initially dislocation slip is governed only by crystal axis orientation, stacking fault energy, i.e. chemical composition of an alloy, and test temperature. Twinning operates only when the stress level exceeds the critical stress for twinning (τ_{tw}). The high carbon content in Hadfield

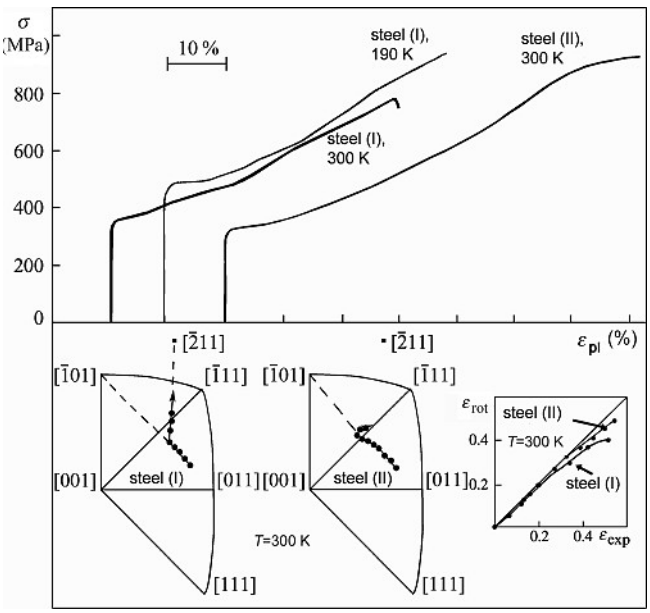

Fig. 5. Stress vs. plastic strain and rotation of crystal loading axis for $[\bar{1}23]$ oriented crystals of steels (I) and (II).

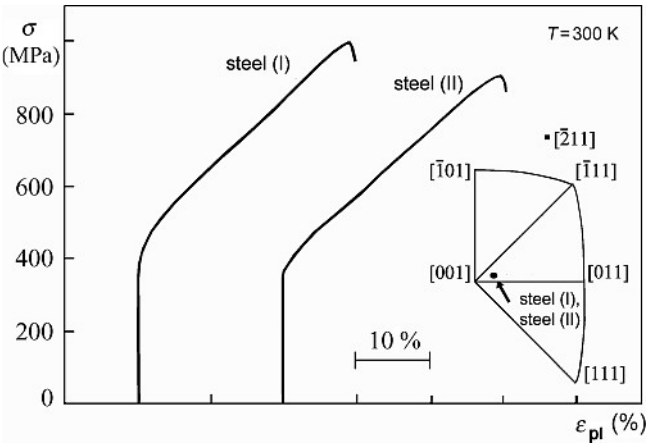

Fig. 6. Stress vs. plastic strain and rotation of crystal loading axis for [001] oriented crystals of steel (I) and (II) at 300 K.

steel provides for significant solid solution hardening so that the stress level is high enough to trigger twinning from the very beginning of plastic flow in favourable orientations. By contrast, substantial strain hardening due to dislocation activity is needed in the case of low-strength alloys in order to reach τ_{tw}. The low stacking fault energy, and the differences in Schmid factors for dislocation slip and twinning (Table 1) provide further rationales for the observed twinning from the onset of deformation in the [$\bar{1}$11] and [011] orientations, as well as the small amount of plastic deformation by dislocation slip prior to twinning in the [$\bar{1}$23] orientation, and dislocation slip in the [001] orientation.

For the first time, mechanical twinning from the very beginning of plastic flow has been observed in fcc single crystals loaded in tension along the [011] axis at $T = 300$ K. Initially, twinning on one primary system is the operative deformation mechanism in these crystals and activation of several twin systems at higher strains results in high values of θ. According to the twin hardening theory [3, 12] the high density of thin twins of several systems provides numerous barriers to the movement of slip dislocations and the high values of the strain hardening coefficient are a result of the interaction of dislocations and twin boundaries.

Alloying of Hadfield steel with aluminium produces an increase in stacking fault energy, which is one of the governing factors of twinning. Consequently, aluminium

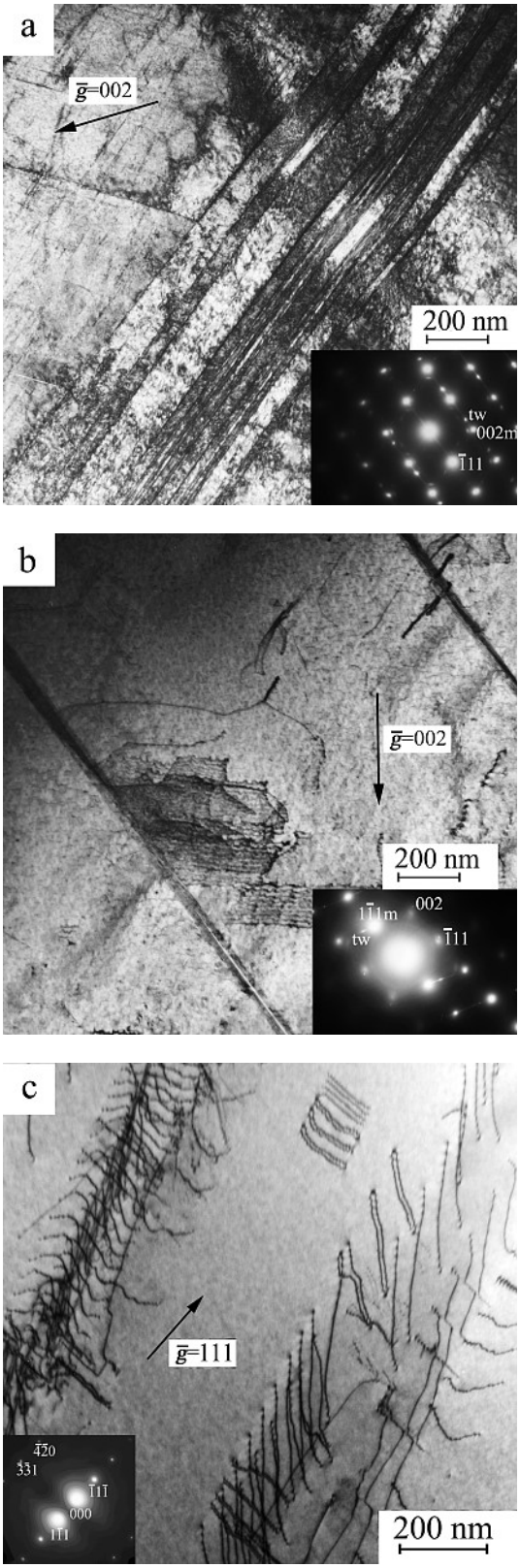

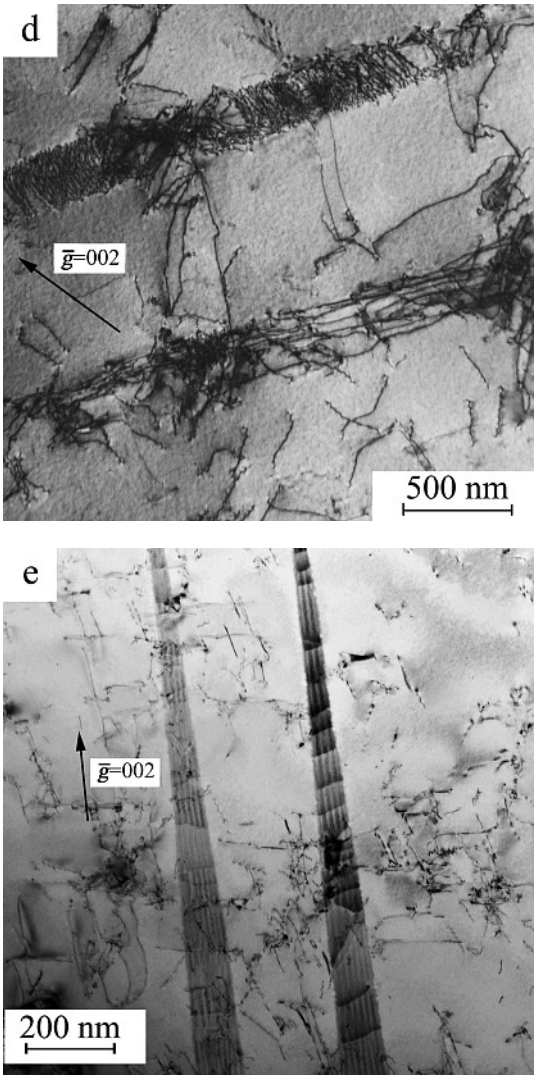

Fig. 7. TEM micrographs of representative microstructures for deformed [$\bar{1}$23] and [001] oriented single crystals of steels (I) and (II). (a) [$\bar{1}$23], steel (I), $\varepsilon_{pl} = 20\,\%$, $T = 300$ K; (b) [$\bar{1}$23], steel (I), $\varepsilon_{pl} = 5\,\%$, $T = 190$ K; (c) [$\bar{1}$23], steel (II), $\varepsilon_{pl} = 5\,\%$, $T = 300$ K; (d) [001], steel (II), $\varepsilon_{pl} = 15\,\%$, $T = 300$ K; (e) [001], steel (I), $\varepsilon_{pl} = 5\,\%$, $T = 300$ K.

moves the onset of twinning to later stages of deformation in [$\bar{1}$11]- and [011]-oriented crystals. As the [$\bar{1}$11] orientation is the one preferred for twinning (Table 1) [12], it starts at strains 5% lower than in the [011] oriented crystals. Another possibility to shift the onset of twinning to higher strains is via a change of initial crystal orientation from [011] to [$\bar{1}$23] in steel (I), and in fact, twinning occurred in [$\bar{1}$23]-oriented crystals only after 20% of plastic deformation. The high strain hardening up to $\varepsilon_{pl} < 20\%$ in steel (I) compared to hardening during dislocation slip in one system in [$\bar{1}$23]-oriented crystals of steel (II) is associated with dislocation slip accompanied by a strain ageing phenomenon. No dislocation pile-ups were found and dislocations were randomly distributed throughout the crystal. The low values of θ observed in steel (II) of [$\bar{1}$23] orientation during the first stage of deformation at $\varepsilon_{pl} < 8\%$ are connected with the development of planar dislocation arrangements, whereas the uniform distribution of perfect dislocation was found to coincide with high values of θ in steel (I) at $\varepsilon_{pl} < 20\%$. Similar results have been obtained for Cu–Zn crystals [13–15]. The dislocation arrangement in pure copper is cellular from the very beginning of plastic flow. Alloying with Zn causes a change to a more planar dislocation arrangement and the strain hardening coefficient θ in crystals oriented for single slip decreases [13–15]. Low γ_{SF} and high friction force τ_F due to short range order usually suppress cross-slip and promote the formation of planar dislocation arrangements. In crystals (I) and (II) the critical resolved shear stresses are close to each other, and γ_{SF} of steel (II) is about two times higher than in steel (I). If the dislocation arrangement is defined by these factors, a cellular dislocation structure should arise in steel (II) and a planar one in steel (I). In Hadfield steel, however, dynamic strain ageing and the high mobility of carbon in steels (I) and (II) make the dislocation-structure-dependence different. The strain-rate dependence β is negative in steel (I) and it has positive values in steel (II) at room temperature [6]. Diffusional activity of carbon atoms is assumed to be lower during deformation of steel (II) at room temperature than upon deformation in steel (I) [5, 6]. It is known [5] that the destruction of the short range order provided by Mn–C pairs during deformation leads to softening of active slip systems, as it is not restored during deformation. Consequently, dislocations initially experience the maximum resistance to their movement. Subsequent dislocations experience lower resistance to their movement in comparison to the first one and dislocation pile-ups are easily formed. By contrast, the high mobility of carbon in steel (I) leads to rapid recovery of short range order upon dislocation movement [5], and thus, the formation of dislocation pile-ups is difficult.

Twinning in the [001] orientation of steel (I) is possible in the case of a change in the sequence of partial Shockley dislocation sequence, i.e. the trailing partial acts as a leading one [9, 11]. Schmid factors of $a/6$ <211> partials, which create intrinsic stacking faults (SF) are $m_{tw} = 0.236$ for twinning and $m_{sl} = 0.41$ for dislocation slip. Therefore twinning with formation of intrinsic SFs cannot be realised due to the low values of the Schmid factor for twinning. However, extrinsic SFs can be produced [9, 11], as the Schmid factor for extrinsic SFs is $m_{extrinsic} = 0.47$, and thus, activation of such a twinning mechanism can be realised in [001]-oriented crystals of Hadfield steel [9, 11].

5. Conclusions

In the present study, single crystals of conventional Hadfield steel (Fe-13Mn-1.3C, wt.%) and a variant alloyed with aluminium (Fe-13Mn-2.7Al-1.3C, wt.%) were studied in order to shed light on the mechanisms governing deformation behaviour. The results obtained may be summarised as follows:

- For the aluminium-free steel, mechanical twinning sets in early on for all crystal orientations when tested at room temperature. This is attributed to the combination of low stacking fault energy ($\gamma_{SF} = 0.030\ J \cdot m^{-2}$) with high carbon content.
- Alloying with aluminium leads to an increase in the stacking fault energy from 0.030 to 0.050 $J \cdot m^{-2}$. This suppresses twinning at the early stages for all crystal orientations, and changes the character of the dislocation arrangements from a uniform distribution of perfect dislocations to a planar dislocation arrangement.
- A decrease in the test temperature results in a shift of the onset of twinning to earlier stages of deformation.

References

[1] P.H. Adler, G.B. Olson, W.S. Owen: Metall. Trans. A 17 (1986) 1725.
[2] K.S. Raghavan, A.S. Sastri, M.J. Marcinkowski: Trans. Metall. Soc. AIME 245 (1969) 1569.
[3] P. Müllner, S. Solenthaler, M.O. Speidel, in: M.H. Yoo, M. Wuttig (Eds.), Twinning in Advanced Materials, The Minerals, Metals and Materials Society, Warrendale, PA (1994) 483.
[4] Y.N. Dastur, W.C. Leslie: Metall. Trans. A 12 (1981) 749.
[5] W.S. Owen, M. Grujicic: Acta Mater. 47 (1999) 111.
[6] B.K. Zuidema, D.K. Subramanyam, W.C. Leslie: Metall. Trans. A 18 (1987) 1629.
[7] R. Berner, H. Kronmüller: Plastische Verformung von Einkristallen, Moderne Probleme der Metallphysik, Bd. 1, Springer-Verlag, Berlin (1965).
[8] P.B. Hirsch, A. Howie, R.B. Nicholson, D.W. Pashley, M.J. Whelan: Electron Microscopy of Thin Crystals, Krieger, Huntington, New York (1977).
[9] Y.I. Chumlyakov, I.V. Kireeva, E.I. Litvinova, E.G. Zakharova, N.V. Luzginova, H. Sehitoglu, I. Karaman: The Physics of Metals and Metallography 90, Suppl. 1 (2000) S1.
[10] E.G. Zakharova, I.V. Kireeva, Y.I. Chumlyakov, S.P. Efimenko, H. Sehitoglu, I. Karaman: Doklady Physics 47 (2002) 515.
[11] I. Karaman, H. Sehitoglu, Y.I. Chumlyakov, H.J. Maier, I.V. Kireeva: Scripta Mater. 44 (2001) 337.
[12] J.W. Christian, S. Mahajan: Progress Mater. Sci. 39 (1995) 1.
[13] D. Kuhlmann-Wilsdorf: Mater. Sci. Eng. A 113 (1989) 1.
[14] D. Kuhlmann-Wilsdorf: Metall. Mater. Trans. A 35 (2004) 369.
[15] S.I. Hong, C. Laird: Acta Metall. Mater. 38 (1990) 1581.

(Received July 21, 2004; accepted November 27, 2006)

Correspondence address

Elena Astafurova
Siberian Physical Technical Institute at Tomsk State University
Novosobornaya sq., 1, 634050 Tomsk, Russia
Tel.: +3822 533 209
Fax: +3822 533034
E-mail: zakharova_e@spti.tsu.ru